1
Epoxy–Vermiculite Nanocomposites

Vikas Mittal

1.1
Introduction

Epoxies form a special class of thermosetting polymeric materials having high thermal and environmental stability. They are well known as creep-resistant materials with very high stiffness properties [1–3]. Owing to these properties, a wide spectrum of epoxy applications is available, which includes the use of epoxies as adhesives, coatings, printed circuit boards, electrical insulators, and so on. One of the major areas where epoxy adhesives find tremendous use are packaging laminates where their sole use is to hold together the various polymeric foils used in these commercial packaging laminates. To save the material costs, an overall decrease in the thickness of the packaging laminate can be achieved if the adhesive can also be made to contribute to the properties required for a packaging material apart from its function of being an adhesive. The common properties required being the permeation barrier, mechanical performance, transparency, suitability for food contact applications, ease of printability, and so on. Permeation barrier to oxygen and water vapor form the most important property needed in the packaging materials. This can be achieved by altering the polymer network structure obtained by crosslinking of the epoxide groups with amines or other crosslinking agents [4, 5]. The use of epoxy polymer with stiff rod-like units in the backbone can help to enhance the required properties. The other alternative includes the incorporation of inorganic fillers in the polymer matrix, this approach being easier to monitor and control. As the filler shape, size, and interfacial interactions affect the polymer properties greatly, organically treated plate-like inorganic aluminosilicate particles can be incorporated in the polymer matrix to achieve polymer nanocomposites for improvement in barrier performance. By incorporating impermeable, transparent, plate-like nanoparticles in the polymer matrix, the permeating molecules are forced to wiggle around them in a random walk, hence diffusing through a tortuous pathway [6–8]. Besides, the decrease in transmission rate of the permeant is a function of the aspect ratio of the inclusions, their volume fraction, and orientation.

The synthesis of epoxy–clay nanocomposites has been extensively studied; however, majority of these studies focused on enhancing the mechanical properties

Thermoset Nanocomposites, First Edition. Edited by Vikas Mittal.

with the incorporation of organically modified fillers [9–17], thus largely neglecting the permeation properties. Only a few recent studies have discussed these properties in detail [18–23]. Apart from that, montmorillonite has been the most commonly used aluminosilicate in these studies. Owing to the low charge density (0.25–0.5 equiv mol^{-1}), a larger area per cation is available on the surface, which leads to a lower basal plane spacing in the clay after surface ion exchange with alkyl ammonium ions. On the other hand, minerals with high charge density (1 equiv mol^{-1}), such as mica, and hence subsequent smaller area per cation, do not swell in water and thus do not allow the cation exchange. However, aluminosilicates with medium charge densities of 0.5–0.8 equiv mol^{-1}, such as vermiculite, offer a potential of partial swelling in water and cation exchange, which can lead to a much higher basal plane spacing in the modified mineral if optimum ion exchange is achieved. In the pristine state, vermiculite particles are composed of stacks of negatively charged 2 : 1 aluminosilicate layers (ca. 0.95 nm thick) with one octahedral sheet sandwiched between two opposing tetrahedral sheets and the resuting regular gap in between (interlayer). The chemical constitution of its unit cell is $(Mg,Al,Fe)_3(Al,Si)_4O_{10}(OH)_2Mg_x(H_2O)_n$ [24, 25]. Due to isomorphic substitutions in the lattice, the layers have permanent negative charges that are compensated mainly by hydrated Mg^{2+} as interlayer cations. Owing to the higher basal plane spacing in the modified mineral, the electrostatic interactions holding the layers together can be expected to be lower than similar montmorillonite counterparts thus increasing the potential of better properties of the hybrid nanocomposites.

The goal of this investigation was to synthesize epoxy–vermiculite nanocomposite coatings and to study their microstructure development as well as their oxygen and water vapor barrier properties in comparison with already reported epoxy–montmorillonite system [18]. Vermiculite platelets modified with two different ammonium ions were prepared for the purpose. The epoxy matrix and the curing agent were chosen to achieve polymer matrix, which meets the requirements of the food and health regulations and has low gas permeability on its own. The nanocomposite coatings were drawn on polyamide and polypropylene substrates and the curing temperatures were kept low in order to avoid the thermal damage to these substrate foils.

1.2 Experimental

1.2.1 Materials

The epoxy resin, bisphenol A diglycidyl ether (4,4′-isopropylidenediphenol diglycidyl ether) with an epoxide equivalent weight 172–176, was supplied by Sigma (Buchs, Switzerland). Tetraethylenepentamine (TEPA) and tetrahydrofuran (THF) were procured from Fluka (Buchs, Switzerland). Benzyldimethylhexadecylammo-

nium chloride (BzC16) was purchased from Acros Organics (Basel, Switzerland). Corona-treated substrate polypropylene (100 µm thick) and polyamide (15 µm thick) foils were supplied by Alcan Packaging (Neuhausen, Switzerland). A surfactant (trade name BYK-307) was used to achieve better wetting and adherence of the neat epoxy coating to the substrate foils and was obtained from Christ Chemie (Reinach, Switzerland). Russian vermiculite with a chemical composition of $(Mg,Al,Fe)_3(Al,Si)_4O_{10}(OH)_2Mg_x(H_2O)_n$ was obtained from Thermax, Greinsfurth, Austria. Benzyl(2-hydroxyethyl)methyloctadecylammonium chloride (BzC18OH) was synthesized by quaternizing the corresponding amine with 1-bromooctadecane as reported earlier [18].

1.2.2
H_2O_2 Treatment

To partially exfoliate the pristine vermiculite, H_2O_2 treatment was performed. Twenty grams of pristine vermiculite mineral was taken in a 2000-ml beaker and 135 ml of H_2O_2 was added to it. The mixture was stirred (glass stirrer) for 5 min at room temperature followed by heating at 50 °C for 10–15 min until the mineral started to foam. The contents were then stirred using a glass rod. The stirring was continued for 15 min with addition of small amounts of water in between to ease the stirring. After 15 min, beaker was removed from the hot plate and was stirred until the mixture stopped foaming. Once the mixture was cooled, it was filtered, washed with water, and finally with methanol and dried under vacuum.

1.2.3
Milling and De-agglomeration

The minerals were wet ground to the desired particle diameter (partially spherical stacks with average particle size of roughly 5 µm) in the wet grinding mill. The grinding operation was performed keeping in mind that only the thickness of the stacks is reduced. For the milling operation, approximately 100 g of the mineral was placed inside the mill. As much as 85 ml of water was subsequently added to the mineral and a homogeneous slurry was generated. It was then milled for 1 h in the milling chamber. The wet slurry was filtered and subsequently washed with methanol. The material was then dried at 70 °C under reduced pressure. The dried powder was sieved in a 160-µm sieve. Particles were also occasionally de-agglomerated by shearing them mechanically in a Teflon vessel containing zirconium oxide beads.

1.2.4
Delamination

In the as-supplied form, vermiculite contained Mg^{2+} ions on the surface. To achieve delamination, 15 g of milled vermiculite was refluxed in 4 M NaCl solution at 170 °C for 12 days followed by filtration and washing with water [26]. The

delamination reaction was repeated twice. The resulting Na–vermiculite was dried at 80 °C under reduced pressure.

1.2.5
Cation Exchange Capacity

The cation exchange capacity (CEC) of vermiculite minerals before, during, and after the delamination process was determined as reported earlier [27]. To measure the CEC, 50 g of 5 mM copper sulfate solution was added to 52.5 g of 5 mM triethylenetetramine solution to generate $Cu(trien)^{2+}$ solution. The extinction coefficient (~4.84) of the solution at 255 nm wavelength was measured on a Cary 1E spectrometer (Varian, Palo Alto, CA). Approximately 20–30 mg of the vermiculite mineral was separately suspended (shaking and sonication) in 15 g of water in a polypropylene vial. To this suspension, 12 g of the $Cu(trien)^{2+}$ solution was added and the mixture shaken for 30 min. The suspension was then centrifuged and the supernatant liquid filtered through a cellulose acetate filter with 0.45 μm pore diameter. The concentration of $Cu(trien)^{2+}$ in the filtrate was measured photometrically and the amount of exchanged ions was calculated.

1.2.6
Ion Exchange and Nanocomposite Preparation

The mineral surface was rendered organophilic by exchanging its surface inorganic Na^+ cations with benzyldimethylhexadecylammonium chloride (BzC16) and benzyl(2-hydroxyethyl)methyloctadecylammonium chloride (BzC18OH). To a heated (70 °C) dispersion of unmodified clay in water and ethanol, a solution of ammonium salt corresponding to 110% of the CEC of the mineral in ethanol was added dropwise and was stirred overnight. The modified clay was filtered and washed repeatedly with hot water–ethanol mixture. For nanocomposite synthesis, the required amounts of modified vermiculite and epoxy resin were calculated on the basis of the desired inorganic volume fraction as reported earlier:

$$M_{OV} = M_V + (M_V \mathrm{CEC} M_{OC})$$

$$M_{EP} = [(M_V V_{EP} \rho_{EP})/(V_V \rho_V)] - (M_V \mathrm{CEC} M_{OC})$$

where M_{OV} is the mass of the modified vermiculite, M_V is the mass of the inorganic aluminosilicate, M_{OC} is the molar mass of the ammonium ion used to modify the vermiculite surface, M_{EP} is the mass of the epoxy resin, V_V is the inorganic volume fraction, ρ_V is the density of sodium vermiculite (2.6 g cm^{-3}), V_{EP} is the epoxy volume fraction, and ρ_{EP} is its density (1.18 g cm^{-3}).

For the composite synthesis, necessary amount of modified montmorillonite was swollen in THF for 2 h followed by sonication (ultrasound horn). The epoxy resin solution was then mixed with the suspension and sonicated. The curing agent, that is, TEPA, was then added and the amine to epoxy mole ratio was maintained at 0.3 : 1. The nanocomposite films were drawn on the corona-treated surface of PP and PA foils with the help of a bar coater (90-μm gap). The coated films were dried at room temperature for 15 min and under reduced pressure for

another 15 min, then cured at 70 °C overnight, and postcured at 90 °C for 4 h. It is worth mentioning here that no sedimentation of the inorganic phase was observed for the time scale of the film preparation. Dry-coated films in the thickness range of ca. 10 μm were achieved, and the correct thickness was determined by weighing the samples in air and in ethanol using an analytical balance (Mettler AE 200) and a homemade device similar to the Mettler density kit ME-33360.

1.2.7 Characterization of the Fillers and Composite Films

The mean particle size was measured by light scattering using Malvern mastersizer. As much as 0.1 g of mineral was suspended in 15 ml of deionized water by shaking and sonication. Polydisperse sample analysis mode was employed and particle density of 2.7 g cm^{-3} was used. Laser beam length of 2.4 mm was selected. The sample presentation unit was filled with about 1000 ml of degassed water. Mineral slurry was then added to the sample presentation unit. The slurry was sonicated again for 10 min before performing the light scattering measurements. Apart from mean diameter $D_{0.5}$, aspect ratio of the minerals (largest dimension to the shortest dimension) was also recorded. It should however be noted that these values are only average values as the particle shapes and sizes had a large distribution. The particle size analyzer visualized the mineral particles as spherical in order to calculate the effective mean diameter. Thus, the calculated mean sizes have contributions from length, breadth, and thickness of the particles.

High-resolution (Hi-Res) thermogravimetric analysis (TGA) of the modified clays, in which the heating rate is coupled to the mass loss, that is, the sample temperature is not raised until the mass loss at a particular temperature is completed, was performed on a Q500 thermogravimetric analyzer (TA Instruments, New Castle, DE). All measurements were carried out under an air stream in the temperature range 50–900 °C.

The oxygen (23 °C and 0% RH) and water vapor (23 °C and 100% RH) transmission rate through substrate foils coated with the neat epoxy and the nanocomposites was measured using OX-TRAN 2/20 and PERMATRAN-W 3/31 (Mocon, Minneapolis, MN), respectively. The PP and PA substrates were selected on the basis of their high transmission rate for the specific permeant so that they do not hinder measuring the permeation through the coated film. The transmission rate was normalized with respect to thickness and an average of five values was reported.

Wide-angle X-ray diffraction (WAXRD) patterns were collected on a Scintag XDS 2000 diffractometer (Scintag Inc., Cupertino, CA) using CuK_α radiation (λ = 0.15406 nm) in reflection mode. The instrument was equipped with a graphite monochromator and an intrinsic germanium solid-state detector. The samples were step scanned (step width 0.02° 2θ, scanning rate 0.06° min^{-1}) at room temperature from 1.5 to 15° 2θ. The (001) basal-plane reflection of an internal standard muscovite (very thin platelets, 2θ = 8.84°) was used to calibrate the line position of the reflections.

The microstructure of the filler in the composite films was studied by bright-field TEM using a Zeiss EM 912 Omega (Leo, BRD) microscope. Small pieces of

coated foils etched with oxygen plasma were embedded in an epoxy matrix (Epon 812 + Durcopan ACM 3:4, Fluka, Buchs, Switzerland) and 50- to 100-nm-thick sections were carefully microtomed with a diamond knife (Reichert Jung Ultracut E). The sections were supported on 100 mesh grids sputter-coated with a 3-nm-thick carbon layer.

1.3 Results and Discussion

On the one hand, as the lateral dimension of the montmorillonite is limited by the weathering and purification operations, the resulting aspect ratio is also limited to lower values. On the other hand, if vermiculite is optimally modified and hence is made to exfoliate in the polymer matrix, a much higher aspect ratio can be generated. As the permeation properties are significantly affected by exfoliated platelets owing to the enhancement of tortuity in the permeant random path through the membrane, better barrier performance can be expected in the vermiculite system. However, the presence of a greater number of cations in a specific area as compared to montmorillonite also makes it difficult to swell and modify and the platelets are held together by much stronger electrostatic forces. Therefore, only a combined effect of these factors can be expected on the final composite properties.

Table 1.1 shows the mean size ($D_{0.5}$) and cation exchange capacity values of the pristine vermiculite along with mineral after milling, de-agglomeration, H_2O_2

Table 1.1 Mean size, aspect ratio, and cation exchange capacity of vermiculite samples after milling (1 h), de-agglomeration, and delamination.

	$D_{0.5}$ (μm)	Aspect ratio	CEC (μeq g^{-1})
Pristine vermiculite			150
Vermiculite milled, fraction <160 μm	36.87	5.21	240
Vermiculite milled, fraction <160 μm, de-agglomerated	23.59 ($D_{0.9}$ 77.99 μm)		242
Vermiculite milled, fraction 160–250 μm	92.87	6.48	
Vermiculite milled, fraction 160–250 μm, re-milled	29.84 ($D_{0.9}$ 101.74 μm) for fraction <160 μm		
Vermiculite milled, fraction <160 μm, H_2O_2 treatment	35.5		300
Vermiculite milled, fraction >160 μm, H_2O_2 treatment	78.23		200
Delaminated vermiculite	34.11	7.5	1440

treatment as well as delamination. The as-received vermiculite mineral had a low CEC value of 150 μeq g^{-1}. The milled vermiculite was sieved and the fraction with <160 μm size was observed to have a mean diameter of 36.9 μm and a CEC of 240 μeq g^{-1}, which was higher than the pristine mineral. However, after de-agglomeration of the mineral, the size was further reduced to 23.6 μm, but a similar CEC value of 242 μeq g^{-1} was observed, which indicated that the de-agglomeration process was not effective. The $D_{0.9}$ value of 78 μm also indicated the broad distribution in particle size. The fraction in the size range of 160–250 μm had a mean diameter of 92.9 μm. A rough estimate of the aspect ratio was also generated with the particle size analyzer, and the vermiculite fraction with <160 μm fraction had an aspect ratio of 5.21 as compared to 6.48 for the fraction >160 μm. Though the higher sized fraction had slightly higher aspect ratio, it was however a result of higher tactoid or stack thickness as well as higher diameter in the mineral. It should also be noted that due to large distribution in the size of the particles, a distribution in the aspect ratio also existed. The fraction in the range of 160–250 μm was re-milled and an average size of 29.9 μm was measured. A much higher diameter $D_{0.9}$ of 101.8 μm for this fraction indicated that the particle size distribution was still broad. In another trial, the hydrogen peroxide-treated vermiculite was milled and a mean size of 35.5 μm was observed for the fraction <160 μm. A cation exchange capacity value of 300 μeq g^{-1} was obtained for this fraction, indicating that the H_2O_2 treatment of vermiculite prior to milling improved the CEC further as compared to both the pristine vermiculite flakes and the milled vermiculite without H_2O_2 treatment. The fraction above >160 μm had mean size of 78.2 μm and its CEC value of 200 μeq g^{-1} was higher than the pristine mineral. The mean size and aspect ratio values of the particles decreased when the milling time was enhanced to 2 h, which indicated that the lateral dimensions of the minerals were impacted by the longer milling periods.

The findings from Table 1.1 confirm that both milling type and time affected the overall dimensions of the mineral particles. Though the mineral particles have average dimensions in the μm scale and various milling and sieving steps lead to minor changes in the overall size, it should be noted that these particles form precursors to the high aspect ratio primary platelets, thus their handling during the milling and de-agglomeration processes has immense significance. Reduction of lateral dimensions signifies reduced aspect ratio, which does not lead to the optimal enhancements in composite properties when such minerals are incorporated into the polymer matrices. It has been often reported that mechanical and permeation properties of the materials are strongly impacted by filler volume fraction as well as aspect ratio. In fact, only exfoliated platelets were reported to contribute to the barrier performance of the polymer-layered silicate nanocomposites [18]. Pretreatment of the pristine minerals (e.g., H_2O_2 treatment) provided additional advantages in achieving the goal of higher aspect ratio minerals. Enhancement of the CEC of the minerals after treatment suggested that higher extent of mineral surface was exposed due to penetration of the H_2O_2 molecules into the mineral interlayers and possibly reduction in the stack thickness as a consequence. Such treatments are also advantageous to remove any impurities present in the minerals.

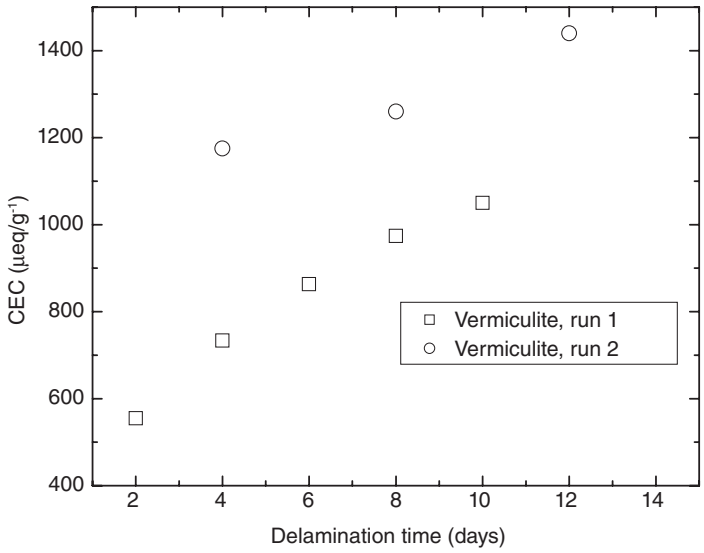

Figure 1.1 CEC values of vermiculite as a function of delamination time with NaCl and $LiNO_3$, respectively.

Figure 1.1 demonstrates the evolution of CEC of vermiculite as a function of number of delamination cycles and delamination time. Vermiculite used for delamination was <160 μm sample, which was treated with H_2O_2 before milling. The first 10 days of delamination of vermiculite with NaCl allowed partial exchange of the Mg^{2+} ions with Na^+ ions generating Na–vermiculite with a CEC of 1050 μeq g^{-1}. Second delamination cycle for further 12 days increased the CEC relatively slowly to 1440 μeq g^{-1}. It signified nearly a tenfold increase in CEC as compared to the pristine mineral. The mean size and aspect ratio of the delaminated minerals in Table 1.1 were similar to the milled materials indicating that although the interlayers were swollen and access to exchangeable cations was enhanced in the delamination process, loose stacks of platelets may still exist. It has also been reported that during the cleaving process, the particle diameter also reduced slightly along with the thickness, thus, justifying the observed values of mean particle size. However, it also confirmed that the mean size of the starting materials was suitable as it allowed the penetration of the NaCl and $LiNO_3$ in the interlayers during the delamination process. Though a partial access was gained to the available surface cations after the cleavage process, the minerals obtained were readily dispersible in water and their enhanced cation exchange capacity was suitable to carry out the surface modification processes to render them compatible with organic polymer matrices.

To achieve compatibility of the mineral and to reduce the surface energy, the sodium ions were exchanged with benzyldimethylhexadecylammonium chloride (BzC16) and benzyl(2-hydroxyethyl)methyloctadecylammonium chloride (BzC18OH).

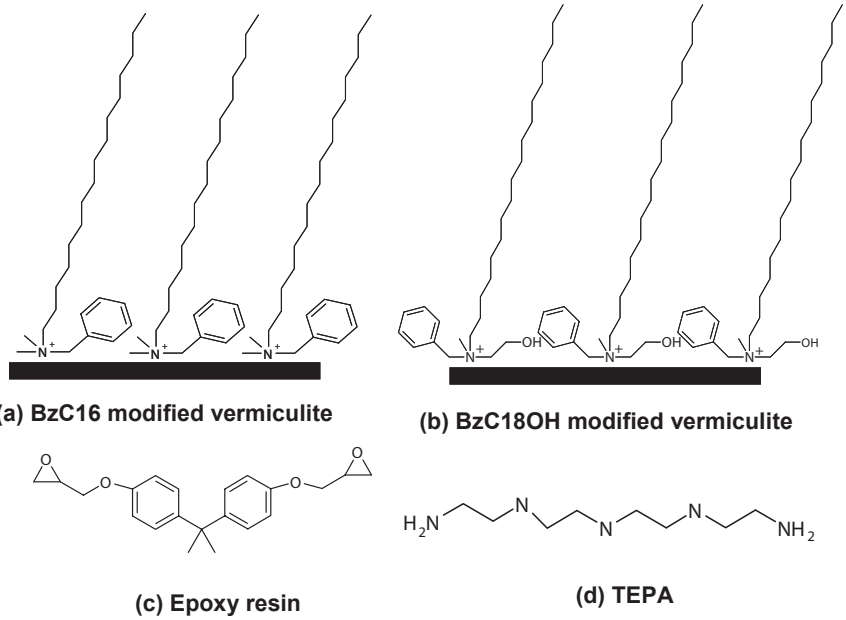

Figure 1.2 (a) and (b) Schematic of modified vermiculites and the chemical architecture of ammonium ions; (c) and (d) chemical structure of the epoxy resin and the crosslinker tetraethylenepentamine.

The two ammonium ions were chosen in order to analyze the effect of different chemical architecture of the ammonium ions on the final composite properties. Depending on the interactions of the swelling solvent and the epoxy prepolymer with the ammonium ion, more chemical interaction of the epoxide groups with the hydroxyl groups present in the ammonium ions can be expected, thus leading to chemical grafting of the epoxy chains on the surface. Similarly, benzyl group present on the surface is also expected to aid in generating stronger van der Waals attraction forces with the epoxy polymer. Figure 1.2 shows the schematic of the modified vermiculites as well as the chemical structures of the system constituents. It is also worth mentioning here that other modifications such as benzyldibutyl(2hydroxyethyl)ammonium chloride, which have been found to significantly exfoliate the montmorillonite clay platelets in the epoxy matrix, were also tried to be exchanged on the vermiculite surface. However, no exchange could be achieved even when the system was constantly stirred for 2 days or higher amounts of ammonium salts corresponding to the mineral CEC were used.

The presence of a local bilayer during the cation exchange was avoided as the presence of excess unattached modifier molecules can negatively interact with the epoxy prepolymer, thus inducing system instability and subsequent loss of composite properties. Figure 1.3 shows the TGA thermograms of the modified vermiculites. Absence of any low-temperature degradation peak in the thermograms

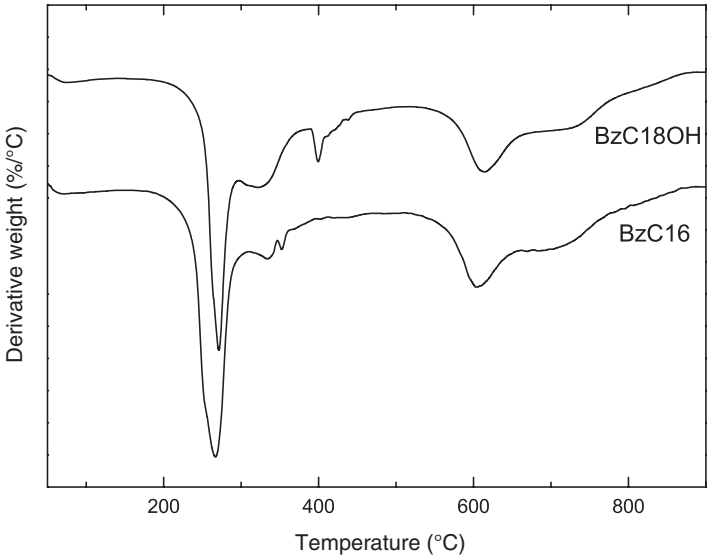

Figure 1.3 TGA thermograms of the surface-modified vermiculites.

Table 1.2 Density of the organo-vermiculites and their 3.5 vol% composites.

Modification	Modified filler	Filler weight	Composite density
	Density (g cm^{-3})	Fraction (%)	(g cm^{-3})
BzC18OH	1.43	11.33	1.20
BzC16	1.53	10.80	1.21

indicates that the excess of the modifier molecules could be successfully washed off. However, it was also important to achieve satisfactory extent of surface ion exchange in order to completely organophilize the mineral. Exchange of >95% of the surface ions was achieved in the present system. As the higher CEC of the mineral leads to the presence of a large number of organic chains on the surface leading to a lower density of the modified vermiculite as compared to the unmodified state, therefore these values should be taken into account for calculating the true volume fraction of the filler. Table 1.2 details these values for the modified filler and the composites. The inorganic volume fraction of 3.5% was used for composites as it was found to be an optimum value for achieving the enhancement in the permeation properties.

The basal plane spacing in the nonmodified vermiculite was found to be 1.22 nm, which was enhanced to 3.25 nm for BzC16-modified vermiculite and 3.40 nm for BzC18OH-modified vermiculite. The absence of the peak corresponding to 1.22 nm

Table 1.3 Basal plane spacing of the fillers, their suspensions, and epoxy composites.

Filler	*d*-spacing filler powder (nm)	*d*-spacing of filler suspended in DMF (nm)	*d*-spacing of filler suspended in DMF + epoxy (nm)	*d*-spacing in epoxy composite (nm)
Na–vermiculite	1.22	1.42	1.42	1.29
BzC18OH	3.40	3.80	3.80	3.96
BzC16	3.25	3.34	3.53	3.68

in the diffractograms of the modified minerals also confirmed that the surface cations were fully exchanged during the exchange process. In contrast, montmorillonite modified with BzC16 and BzC18OH had, respectively, the basal plane spacing of 1.87 and 2.06 nm [18]. It clearly indicates that owing to higher CEC (880 $\mu eq\, g^{-1}$ for montmorillonte), the platelets were pushed to much larger distances in vermiculite than in montmorillonite for the same ammonium ions exchanged on the surface. Table 1.3 describes the basal plane spacing values of the dry fillers, the suspension of fillers in DMF, the suspension of fillers in DMF and epoxy prepolymer, and the final composites. DMF has been chosen for these experiments because of its low volatility for the time scale of the X-ray scanning experiments. The presence of an X-ray peak in the solvent suspensions of modified fillers indicates that the fillers were not completely exfoliated in the solvent itself indicating the presence of residual electrostatic forces. The suspensions of fillers in solvent and prepolymer also confirmed that the prepolymer itself was also unable to delaminate the platelets, although there was no decrease in the basal plane spacing as sometimes observed in the montmorillonite system. However, no change in the basal plane spacing on the addition of prepolymer would suggest that no or very weak intercalation of the prepolymer took place. The basal spacing was enhanced to some extent after curing and nanocomposite generation indicating that intercalation occurred during the polymerization leading to further pushing apart of the platelets. However, the presence of diffraction peak in the composite diffractograms also indicated that full exfoliation of the platelets could not be achieved indicating the presence of residual attraction forces. Figures 1.4 and 1.5 show the X-ray diffractograms of the modified fillers and their 3.5 vol% composites. As it is evident from the diffractograms that the intensity of the diffraction peak was reduced after incorporation in the polymer, but owing to the dependency of the intensity on sample preparation and mineral defects, the analysis of the microstructure of the composites was also performed by TEM. Figure 1.6 shows the TEM micrographs of the 3.5 vol% composites. The micrographs showed the presence of mostly mixed morphology with single layers and intercalated tactoids of varying thicknesses. The platelets were also observed to be bent and folded and no specific alignment of the tactoids could be observed at any magnification. One should also note here that the misalignment of platelets leads

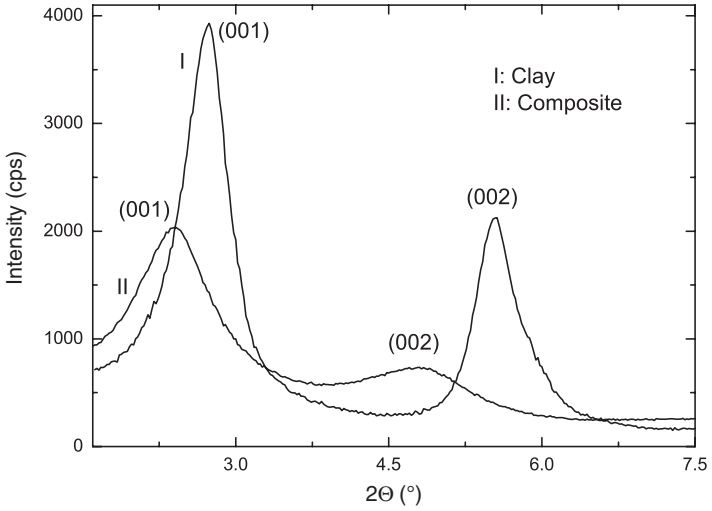

Figure 1.4 X-ray diffractograms of the (I) BzC16-modified vermiculite and (II) the filler in epoxy composite.

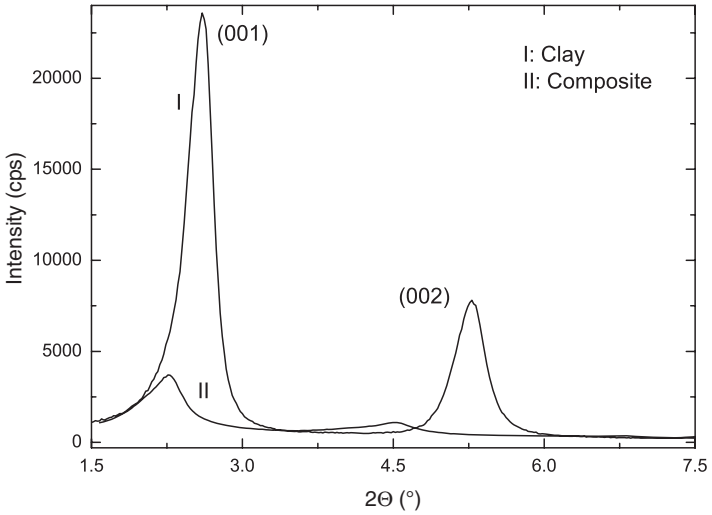

Figure 1.5 X-ray diffractograms of the (I) BzC18OH-modified vermiculite and (II) the filler in epoxy composite.

to reduction in the composite properties, especially gas permeation properties. It has been recently reported by using finite element models of the misaligned platelets that the completely misaligned platelets (as seen in the current system) are roughly one-third effective as barrier materials as compared to the completely aligned platelets thus confirming the need to generate more alignment [28]. The

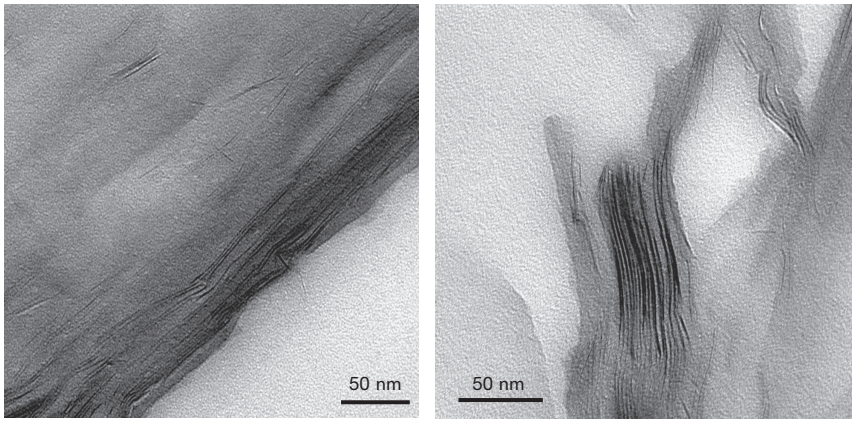

Figure 1.6 TEM micrographs of the 3.5 vol% (a) BzC16–vermiculite epoxy and (b) BzC18OH–vermiculite epoxy composites. The dark lines are cross-sections of aluminosilicate platelets.

Table 1.4 Oxygen and water vapor transmission rates through 3.5 vol% organo-vermiculite nanocomposites at 23 °C.

Composite	Oxygen permeability coefficient[a)]	Water vapor transmission rate[a)]
	cm^3 μm/(m^2 d mmHg)	g μm/(m^2 d mmHg)
Neat epoxy	2.0	10.0
Na–vermiculite	1.7	37.0
BzC18OH	1.5	7.5
BzC16	1.4	9.7

a) Relative probable error 5%.

TEM micrographs not only confirmed the X-ray findings about the intercalated morphology, but also showed the presence of some exfoliated layers totally missed in the WAXRD.

The gas permeation properties through the composite films containing 3.5% filler volume fraction were measured and are reported in Table 1.4. The oxygen permeation through the pure epoxy films was recorded as 2 cm^3 μm/(m^2 d mmHg), which in itself is much lower than the other adhesives used in the packaging laminates. The oxygen permeation through BzC18OH and BzC16 composites was,

respectively, observed as 1.5 and 1.4 cm^3 μm/(m^2 d mmHg), which indicates that in spite of very high oxygen resistance of the matrix, further improvements in the oxygen barrier performance could be achieved by the incorporation of the nanoplatelets. These values for the montmorillonite fillers were reported as 2.2 and 1.6, respectively. It also indicates that the oxygen permeation was unaffected by the chemical nature of the ammonium ion exchanged on the surface and relied more on the polymer filler interactions. The water vapor permeation through the composite films with unmodified vermiculite was observed to be 37 gμm/(m^2 d mmHg), which was much higher than 10 gμm/(m^2 d mmHg) observed for the pure polymer itself. A value of 7.5 and 9.7 gμm/(m^2 d mmHg) was observed for the BzC18OH and BzC16 composites, respectively, indicating that the polarity of the hydrophilic interlayers was significantly reduced after the cation exchange, but interlayers are still partially polar to attract the molecules of water. Thus the composite properties can be represented as a combined effect of positive factors such as potential higher aspect ratio of the platelets, intergallery polymerization, and enhanced basal plane spacing as well as negative factors such as residual electrostatic forces. Thus, attaching much longer alkyl chains as well as increasing the grafting density in the ammonium ions could be expected to further eliminate the electrostatic interactions.

1.4 Conclusions

Vermiculite platelets modified with alkyl ammonium ions contained much higher basal plane spacing than the modified montmorillonites. The clay interlayers were further pushed apart in the composites owing to interlayer polymerization and the polymer chains were not squeezed out during solvent evaporation and curing. However, just having large d-spacing does not constitute the sole requirement for filler exfoliation, because owing to higher number of cations available per unit area in vermiculite, the residual electrostatic forces were still present although the area is covered with a large number of chains. The oxygen permeation through the composite films was further reduced by 30% in 3.5 vol% BzC16 composites, even though the permeation through the pure matrix was also very low. Owing to the polar interlayers, the water vapor permeation through the nonmodified vermiculite composites exponentially increased, which was significantly reduced in modified vermiculite composites. Grafting of large alkyl chains and ammonium ions with higher chain densities can be a possible approach to further reduce the electrostatic forces in these high CEC minerals.

Acknowledgment

Major portion of the presented work has been published in *Journal of Composite Materials*, 2008, 42, 2829, copyright Sage Publishers.

References

1 May, C.A. (1988) *Epoxy Resins Chemistry and Technology*, 2nd edn, Dekker, New York.
2 Lee, H. and Neville, K. (1967) *Handbook of Epoxy Resins*, McGraw-Hill, New York.
3 Ellis, B. (1993) *Chemistry and Technology of Epoxy Resins*, Blackie Academic & Professional, London.
4 Silvis, H.C. (1997) Recent advances in polymers for barrier applications. *Trends Polym. Sci.*, **5** (3), 75–79.
5 Brennan, D.J., Haag, A.P., White, J.E., and Brown, C.N. (1998) High-barrier poly(hydroxy amide ethers): effect of polymer structure on oxygen transmission rates. 2. *Macromolecules*, **31** (8), 2622–2630.
6 Gusev, A.A. and Lusti, H.R. (2001) Rational design of nanocomposites for barrier applications. *Adv. Mater.*, **13** (21), 1641–1643.
7 Eitzman, D.M., Melkote, R.R., and Cussler, E.L. (1996) Barrier membranes with tipped impermeable flakes. *AIChE J.*, **42** (1), 2–9.
8 Fredrickson, G.H. and Bicerano, J. (1999) Barrier properties of oriented disk composites. *J. Chem. Phys.*, **110** (4), 2181–2188.
9 Messersmith, P.B. and Giannelis, E.P. (1994) Synthesis and characterization of layered silicate–epoxy nanocomposites. *Chem. Mater.*, **6** (10), 1719–1725.
10 Lan, T., Kaviratna, P.D., and Pinnavaia, T.J. (1995) Mechanism of clay tactoid exfoliation in epoxy–clay nanocomposites. *Chem. Mater.*, **7** (11), 2144–2150.
11 Zilg, C., Mulhaupt, R., and Finter, J. (1999) Morphology and toughness/stiffness balance of nanocomposites based upon anhydride-cured epoxy resins and layered silicates. *Macromol. Chem. Phys.*, **200** (3), 661–670.
12 Brown, J.M., Curliss, D., and Vaia, R.A. (2000) Thermoset-layered silicate nanocomposites. Quaternary ammonium montmorillonite with primary diamine cured epoxies. *Chem. Mater.*, **12** (11), 3376–3384.
13 Zerda, A.S. and Lesser, A.J. (2001) Intercalated clay nanocomposites: morphology, mechanics, and fracture behavior. *J. Polym. Sci. Part B: Polym. Phys.*, **39** (11), 1137–1146.
14 Kornmann, X., Lindberg, H., and Berglund, L.A. (2001) Synthesis of epoxy–clay nanocomposites: influence of the nature of the clay on structure. *Polymer*, **42** (4), 1303–1310.
15 Kornmann, X., Thomann, R., Mulhaupt, R., Finter, J., and Berglund, L. (2002) Synthesis of amine-cured, epoxy-layered silicate nanocomposites: the influence of the silicate surface modification on the properties. *J. Appl. Polym. Sci.*, **86** (10), 2643–2652.
16 Kong, D. and Park, C.E. (2003) Real time exfoliation behavior of clay layers in epoxy–clay nanocomposites. *Chem. Mater.*, **15** (2), 419–424.
17 Chin, I.J., Thurn-Albrecht, T., Kim, H.C., Russell, T.P., and Wang, J. (2001) On exfoliation of montmorillonite in epoxy. *Polymer*, **42** (13), 5947–5952.
18 Osman, M.A., Mittal, V., Morbidelli, M., and Suter, U.W. (2004) Epoxy-layered silicate nanocomposites and their gas permeation properties. *Macromolecules*, **37** (19), 7250–7257.
19 Triantafyllidis, K.S., LeBaron, P.C., Park, I., and Pinnavaia, T.J. (2006) Epoxy-clay fabric film composites with unprecedented oxygen-barrier properties. *Chem. Mater.*, **18**, 4393–4398.
20 Xu, R., Manias, E., Snyder, A.J., and Runt, J. (2001) New biomedical poly(urethane urea)-layered silicate nanocomposites. *Macromolecules*, **34** (2), 337–339.
21 Tortora, M., Gorrasi, G., Vittoria, V., Galli, G., Ritrovati, S., and Chiellini, E. (2002) Structural characterization and transport properties of organically modified montmorillonite/polyurethane nanocomposites. *Polymer*, **43** (23), 6147–6157.
22 Chang, J.H. and An, Y.U. (2002) Nanocomposites of polyurethane with various organoclays: thermomechanical properties, morphology and gas permeability. *J. Polym. Sci. Part B: Polym. Phys.*, **40** (7), 670–677.

23 Osman, M.A., Mittal, V., Morbidelli, M., and Suter, U.W. (2003) Polyurethane adhesive nanocomposites as gas permeation barrier. *Macromolecules*, **36** (26), 9851–9858.
24 Jasmund, K. and Lagaly, G. (1993) *Tonminerale und Tone*, Steinkopff-Verlag, Darmstadt.
25 Brindley, G.W. and Brown, G. (1980) *Crystal Structure of Clay Minerals and their X-Ray Identification*, Mineralogical Society, London.
26 Osman, M.A. (2006) Organo-vermiculites: synthesis, structure and properties. Platelike nanoparticles with high aspect ratio. *J. Mater. Chem.*, **16** (29), 3007–3013.
27 Osman, M.A. and Suter, U.W. (2000) Determination of the cation-exchange capacity of muscovite mica. *J. Colloid Interface Sci.*, **224** (1), 112–115.
28 Osman, M.A., Mittal, V., and Lusti, H.R. (2004) The aspect ratio and gas permeation in polymer-layered silicate nanocomposites. *Macromol. Rapid Commun.*, **25**, 1145–1149.